A Difference Imaging Method for Extracting Light Echo Fluxes with an Application to SN 1987A

A. Newman

Department of Physics

Washington University in St. Louis

abnewman@wustl.edu

A. Rest

Cerro Tololo Inter-American Observatory (CTIO), La Serena, Chile

ABSTRACT

A new technique for extracting fluxes from light echoes is presented. Rather than relying on a single template image with no light echo flux, we contruct difference images from every pair of observations. From this, the NN2 method of Barris et al. (2005) is used to compute for each pixel the relative fluxes at each epoch. Statistical methods are presented to calculate the zero-flux level and thus the absolute flux, as well as to detect light echo regions in the resultant images. The technique is applied to the light echoes around SN 1987A, and the images obtained reveal remarkable new detail and structure. Basic geometric properties of the rings are calculated and found to be in agreement with the literature.

Subject headings: methods: data analysis, techniques: photometric, supernova remnants, Magellanic Clouds, ISM: individual (SN 1987A)

1. Introduction

Light echoes offer a wealth of information about their progenitors and their environment. By observing light echoes, it is possible to infer information about the structure and composition of circumstellar matter and the interstellar medium (Xu et al. 1995). Light echoes provide a laboratory for studying important stages in stellar evolution, such as supernovae and variable eruptions, even at much later epochs (Rest et al. 2005b; Tylenda et al. 2005). Although much can be gleaned from the dynamical evolution of a light echo only, absolute surface brightness measurements can provide more detailed information, including independent distance measurements and dust density estimates. This data, however, has been difficult to obtain, principally due to the low brightness of the echoes.

Difference imaging is necessary to observe light echos, but this technique can reveal only the relative fluxes at two epochs. If an image earlier than the light echo event is available, it may be used as a template and subtracted from images at later epochs to determine the light echo flux. Often, however, such an image is not available. Even if such a template image can be constructed, as attempted by Xu et al. (1995), imperfections in the template will propagate through all stages of analysis. In this paper, we present an application of the NN2 algorithm of Barris et al. (2005) to calculate the relative light echo fluxes without the need for a choosing a single, preferred template image. With this technique, images from all epochs are considered equally. We also present a statistical method for estimating the zero-flux level and thus the absolute flux, as well as a method for detecting light echo regions. The entire procedure is tested on light echoes fron SN 1987A, and the resulting images reveal intricate detail. Finally, a basic analysis of the geometry of the light echo rings is presented.

2. Observations

To test the ability of the NN2 algorithm to accurately recover light echo fluxes, light echoes from SN 1987A were chosen for analysis. These are well-studied, in part because they reveal the dust structure of 30 Doradus, an active star-forming region. Thus the results here can be compared to those in the literature. Additionally, these echoes expand quickly enough that there should be no pixels which contain light echos at all epochs, which poses problems for zero-flux level determination, as will be discussed later.

Observations were performed by the SuperMACHO survey on the Cerro Tololo Inter-American Observator (CTIO) Blanco 4m telescope. Imaging was performed every other night in dark time during the months of October, November, December, and January, with occassional images from September and February, during 5 seasons from 2001 through 2005. These are the months in which the Large Magellanic Cloud (LMC) is most visible from Cerro Tololo. We use the $8K \times 8K$ MOSAIC II CCD imager with a FOV of 0.33 square degree, along with a custom broadband VR filter from 500nm to 750nm. For more information on the observation program, see Rest et al. (2005a). For this study, 52 epochs were chosen, with the earliest in 2001 and the latest in 2005. These were selected based on seeing conditions, as measured by the zero-point magnitude and average FWHM and eccentricity of the point-spread functions, and based on their temporal spacing. Data for the 52 selected images are shown in table 1.

3. Analysis

Images from the $N = 52$ epochs considered in this study were first reduced by the SuperMACHO pipeline. The reduction include bias correction, crosstalk elimination, flat fielding, calculation of coordinate system information, deprojection of the image onto the tangential plane, and `dophot`

photometry to compute the zero-point magnitude. The principal feature of the NN2 method is that we consider difference images created from all $N(N-1)/2$ pairs of images. The SuperMACHO pipeline was used to produce the 1326 difference images which served as the input to the NN2 algorithm. The difference images are created by matching point-spread functions. A spatially-varying kernel is convolved with the better image until a good fit with the worse is achieved. Pixel values are then subtracted.

3.1. NN2

The NN2 method was created by Barris et al. (2005) to construct optimal light curves for point-source variable objects from a series of observations. To apply this technique to light echoes, we first consider a single pixel. The presentation below follows that of Barris et al. Let A be the antisymmetric matrix for which A_{ij} is flux in the difference image between epochs j and i. This flux is normalized to zero-point magnitude 30, based on the average zero-point magnitudes of the images at epochs j and i. The matrix A represents the input from the difference imaging pipeline. We attempt to represent A as a vector difference $A_{ij} = V_j - V_i$ by minimizing

$$\chi^2 = \sum_{i<j} \frac{(-A_{ij} + V_j - V_i)^2}{E_{ij}^2} + \frac{\sum V_i}{\langle E \rangle^2}, \tag{1}$$

where E_{ij} represents the error in A_{ij} and $\langle E \rangle$ represents an average error, such as

$$\frac{1}{\langle E \rangle^2} = \frac{2}{N(N-1)} \sum_{i<j} \frac{1}{E_{ij}^2}. \tag{2}$$

The second term in equation (1) is necessary to obtain a unique solution for V, the vector of relative fluxes at each epoch, which is otherwise insensitive to the addition of a constant vector. This term implies $\sum V_i = 0$ and requires us to determine the zero-flux level separately. As derived in Barris et al., χ^2 is minimized by solving the N linear equations

$$\sum_{i;i\neq k} \frac{A_{ik}}{E_{ik}^2} = \sum_i C_{ik} V_i, \tag{3}$$

where

$$C_{ik} = -\frac{1}{E_{ik}^2} + \sum_j \frac{1}{E_{kj}^2} \delta_{ik} + \frac{1}{\langle E \rangle^2}. \tag{4}$$

Uncertainties are obtained from the square roots of the diagonal elements of the matrix (C_{ik}). These uncertainties reflect the imperfect fitting of A as a vector difference. We call this the *internal* error. Additionally, there are uncertainties in V due to errors in the input data A, which we call the *external* error. To estimate the external error in V, we assume that the error E_{ij} in the difference image arises from errors σ_i and σ_j in the original images at epochs i and j, i.e. that there exists a vector σ such that

$$E_{ij}^2 = \sigma_i^2 + \sigma_j^2. \tag{5}$$

To calculate the best-fit σ, we attempt to minimize

$$\chi_e^2 = \sum_{i,j;i<j} \left(-1 + \frac{\sigma_i^2}{E_{ij}^2} + \frac{\sigma_j^2}{E_{ij}^2} \right)^2 . \tag{6}$$

This occurs when

$$\begin{aligned} 0 &= \frac{\partial \chi_e^2}{\partial \sigma_k^2} \\ &= 2 \sum_{i,j;i<j} \left(-1 + \frac{\sigma_i^2}{E_{ij}^2} + \frac{\sigma_j^2}{E_{ij}^2} \right) (\delta_{ik} + \delta_{jk}) \frac{1}{E_{ij}^2} \\ &= 2 \sum_{i;i\neq k} \left(-1 + \frac{\sigma_i^2}{E_{ik}^2} + \frac{\sigma_k^2}{E_{ik}^2} \right) \frac{1}{E_{ik}^2}. \end{aligned} \tag{7}$$

This system of N linear equations may be solved by inverting the matrix D,

$$\sum_{i;i\neq k} \frac{1}{E_{ik}^2} = \sum_i D_{ik} \sigma_i^2, \tag{8}$$

where

$$\begin{aligned} D_{ik} &= \frac{1}{E_{ik}^4}, \quad i \neq k \\ D_{kk} &= \sum_{i;i\neq k} \frac{1}{E_{ik}^4}. \end{aligned} \tag{9}$$

In rare cases, this method yields negative solutions for σ_i^2, indicating that the original assumption that E_{ij}^2 can be well-represented by $\sigma_i^2 + \sigma_j^2$ is not accurate. In practice, this occurs in of order 1 in 10^5 pixels, which are therefore simply masked. The approach given here for calculating the external error is that adopted in the code of Wood-Vasey, Tonry, and Novicki.[1] It differs from that outlined in Barris et al., in which the quantity to be minimized is given as

$$\chi_e^2 = \sum_{i,j;i<j} (-E_{ij}^2 + \sigma_i^2 + \sigma_j^2)^2. \tag{10}$$

The difference is that in equation (6), we seek to minimize the fractional error in the representation of E_{ij} by σ, whereas in equation (10), we seeks to minimize the absolute error. In practice, the errors obtained are similar when both methods are available, but the method presented in Barris et al. fails far more often (i.e., yields negative values for σ_i^2).

To compute the total error, the contributions of both the internal and external errors must be considered. To combine these errors, we adopt the approach of Barris et al. The internal error is scaled as follows:

$$\tau_k = \left(C_{kk}^{-1} \frac{\chi^2}{N_{\rm dof}} \right)^{1/2}, \tag{11}$$

[1] http://ctiokw.ctio.noao.edu:8080/Plone/essence/Software/NN2

where

$$N_{\rm dof} = \frac{N(N-1)}{2} - (N-1) \tag{12}$$

is the number of degrees of freedom. The total error is the quadrature sum of τ and σ. When A is well-represented as a vector difference, $\chi^2/N_{\rm dof} \ll 1$, and the total error is due mainly to the external error. If, on the other hand, $\chi^2/N_{\rm dof} \gg 1$, this factor will correct τ and provide a reasonable total error.

The software to perform the NN2 calculations was written in Python. The heart of the calculation, the `antivec` function, was adapted from the code of Wood-Vasey, Tonry, and Novicki. A region of specified size is read into memory from each of the $N(N-1)/2$ difference images. For each pixel, masked data are discarded as follows. The number of images associated with each epoch (either as the image or template date) in which the pixel is masked is calculated. All images associated with the epoch with the highest count are discarded, and the process is repeated until no masked data remains. (We consider input pixels as masked if they are marked by the SuperMACHO pipeline as saturated.) The NN2 algorithm is run with the remaining data, and a crude zero-flux level is set by shifting the relative fluxes so that the minimum value is 0. Image files containing the flux, internal error, external error, and total error are created. Additionally, mask files are created for each epoch showing which pixels were discarded. Pixels which encountered an error in calculating the external error are also flagged. From these images an image was created indicating the total number of epochs included in the calculation for each pixel. Pixels calculated with fewer than 30 epochs were then masked.

The calculations involve several matrix inversions and are naturally slow. We developed scripts to split the calculations among several processes which could be split among a 20 CPU cluster. The output from these processes was then reassembled into the final images. For 52 images of dimensions 4160×1100, this procedure still required 30 hours. In our experience, speed improvements of a factor 10-100 can be expected from C code.

3.2. Zero flux level

Because the NN2 algorithm provides only relative fluxes, it is necessary to estimate the epochs which contain zero flux for each pixel. A crude estimate is performed by subtracting from each pixel the lowest value obtained at any epoch. Next, the output images from the NN2 program are smoothed by replacing each pixel with the weighted mean of its unmasked neighbors in an 3×3 box centered at the pixel, excluding the highest and lowest fluxes when at least 6 epochs are available. Error images are also created containing the uncertainties in these means. Smoothing reduces the noise in the image and makes the determination of the zero-flux epochs less sensitive to outlier epochs in individual pixels.

To determine the epochs of zero flux for a given pixel, the smoothed fluxes and errors for each epoch are loaded and binned into seasons. The weighted mean of each season is calculated,

excluding the highest and lowest fluxes if at least 6 are available, and a sigma cut is performed in which seasons more than 3 σ above the minimum mean are excluded. In practice, most seasons which will be cut are excluded here. Next, seasons which exhibit a gradient are excluded. This is done by calculating the ratio of χ^2 for the best-fit line, as determined by the least-squares method, to χ^2 for the mean. Seasons for which this ratio exceeds 10 are excluded. Finally, seasons with a normalized χ^2 greater than 3.5 are excluded. The remaining seasons are deemed to represent the zero flux.

To calculate the zero-flux level, the unsmoothed fluxes and errors are loaded, and the mean of each zero-flux season is computed in the same manner as above. The weighted mean of the season means is then calculated. This value is subtracted from every epoch, and the errors are propagated. Sample light curves for pixels with strong and weak light echoes which have been zero-flux corrected are shown in figures 4 and 5.

This procedure is dependent on the availablity of true zero-flux epochs in the neighborhood of every pixel. If used to study light echoes for which only a small range of epochs (relative to the expansion velocity) is available, it will identify the epochs of lowest flux as representing zero flux and thus underestimate the true flux, though still providing a lower limit. This is not an issue in the study of SN 1987A. Its echoes move sufficiently quickly that over a 5 year period, very few, if any, pixels are always illuminated.

3.3. Light echo detection

To assist in seperating light echo pixels from the sky background, the NN2 images from each season were mean combined, excluding the epochs of highest and lowest flux for each pixel with at least 6 unmasked epochs available, resulting in 5 stacked images. Error and mask images were created as well. Since the flux can change by a factor of 2 or more within a single season in a region with a moving light echo, this binning is too coarse to provide useful flux information. It does, however, improve the visibility of faint rings for detection. To further improve visibility, the 5 stacked images were smoothed using the technique described in section 3.2.

Each of the stacked images was analyzed for light echo detection by a series of statistical cuts. Masked pixels and 3×3 regions around bright star centers (defined as stars with a signal-to-noise ratio of 10 or more, as calculated by `dophot`) were excluded first. Pixels with fluxes more than 3 σ above the global mean were then identified as light echo candidates, and the mean sky background was computed. Pixels with fluxes less than 2 σ above this mean were then cut.

The resulting image contains much light echo structure but also many isolated regions of noise. It is desirable to exclude these isolated regions without excluding faint echos, which often are detected as a dense area of small, non-contiguous regions. To do so, the detection scheme was biased toward arc regions, the most probable light echo candidates, by creating an arc assocation map. Arclet regions with a radial thickness of 9 pixels and an arc length of 60 pixels were identified by

starting with a ring centered at the supernova with radius 100 pixels and successively incrementing the radius by 6 pixels. Around each circle, the arclet regions overlap by half with their neighbors. Within each arclet so identified, the density of light echo candidates was calculated. Since the arclets overlap, each pixel is assigned the greated density achieved by any of the arclets to which it belongs. A sample arc density map is shown in figure 6. Pixels with densities greater than 0.2 are deemed to be in a strong arc association and are protected from future cuts.

Next, a neighbor cut was performed, in which pixels with fewer than 50% light echo candidates within a 7×7 pixel box centered on them are excluded. (Masked pixels and pixels excluded by the bright star cut are not included in this box.) This cut was iterated 10 times. This procedure is successful in eliminating almost all of the remaining noise while preserving faint echoes which have been found to lie in arc assocations.

4. Discussion

Images from each step of the image analysis are shown in figures 1 and 2. Figure 1 shows a region of bright rings with complicated structure. Figure 2 shows fainter rings, barely visible in the original difference images, which our technique brings out clearly. A larger field of view is shown in figure 3. Our images clearly show large arcs of a third ring between the bright two inner rings and the fourth outer ring discovered by Xu et al. (1994). We have made a preliminary study of the geometry of the dust illuminated by the light echoes of SN 1987A as follows. For the 2001-2002 season, rings 1, 2, 3, and 4 were hand-selected from the light echo detector output. The echoes were sliced into 3° sectors of a circle centered at the central star. Within each sector, the mean radius in pixels, weighted by fluxes from the season mean-combined image, was calculated. This was converted to a projected radius ρ by adopting a distance of 51.2 kpc to the LMC (Panagia et al. 1991). The distance from the echoing dust to the supernova may then be calculated by

$$z = \frac{\rho^2}{2ct} - \frac{ct}{2} \tag{13}$$

(Sugerman 2003), where we take t to be the time between the maximum V band brightness of SN 1987A and the mean date of the epochs used in the 2001-2002 season. From this we obtain how the distance of the echoing dust in front of SN 1987A varies with position angle. The result is shown in figure 7. At the time of this writing, only amplifier 15 from field sm77 of the SuperMACHO dataset had been fully processed according to the method of this paper. This amplifier contains many light echo regions, but the upper and lower arcs are located in amplifiers 16 and 14, respectively. Therefore there are a number of angular gaps in figure 7, especially in the outer rings. The mean values of ρ and z, calculated from the 3° sectors, are shown in table 2. They are in agreement with the data for the four dust structures described in Xu et al. (1995). However, we are able to detect a greater extent of the outer rings. Hand measurement of an arclet of ring 4 in the southwestern quadrant gives $\rho = 106$ pc. Using this value in equation (13), we find that this ring is illuminated

dust more than 1.2 kpc in front of the SN 1987A. We have also detected light echo arcs within ring 1 which reveal dust only 16 pc in front of the supernova.

Much more challenging than detecting measuring the geometric properties of the echoes is obtaining accurate absolute fluxes. In our season mean-combined images, the brightest knots have a surface brightness of 19.6 mag arcsec^{-2}, in excellent agreement with what we expect based on the difference images. Light echo features with peak surface brightnesses of 25.0 mag arcsec^{-2} are clearly visible. Average surface brightnesses are much lower.

5. Conclusions

The technique presented here is successful in creating detailed maps of the light echoes around SN 1987A. We have identified numerous rings and arc regions, some new. Future work will focus on identifying arcs in a more refined way and making detailed measurements of their geometry and evolution. This will allow determination of the position and inclination of the dust regions illuminated by the light echoes. We will also present surface brightness maps, which can be used to calculate the absolute densities of the dust regions.

Applications of this technique to more complicated light echo structures remain to be done. The method outlined in this paper may be used to help disentangle the echoes arising from multiple dust shells or other complex dust structures suspected to surround other stars in the LMC with light echoes identified from the SuperMACHO survey (e.g. Rest et al. 2005b).

6. Acknowledgments

The SuperMACHO survey is being undertaken under the auspices of the NOAO Survey Program. We are very grateful for the support provided to the Survey program from the NOAO and the National Science Foundation We are particularly indebted to the scientists and staff at the Cerro Tololo Interamerican Observatory for their assistance in helping us carry out the SuperMACHO survey. We also appreciate the invaluable help of Mr. Chance Reschke in building and maintaining the computing cluster we use for image analysis. This project works closely with members of the ESSENCE supernova survey, and we are grateful for their input and assistance.

The support of the McDonnell Foundation, through a Centennial Fellowship awarded to C. Stubbs, has been essential to the SuperMACHO survey. We are most grateful for the Foundation's support for this project.

Drew would like to thank Armin for his mentoring and guidance, Stella for directing a wonderful REU program, and his fellow REU/PIAers for their friendship and all the good times.

REFERENCES

Barris, B. J., Tonry, J. L., Novicki, M. C., & Wood-Vasey, W. M. 2005, AJ, 130, 2272

Panagia, N., Gilmozzi, R., Macchetto, F., Adorf, H.-M., & Kirshner, R. P. 1991, ApJ, 380, L23

Rest, A., et al. 2005a, ApJ, 634, 1103

Rest, A., et al. 2005b, Nature, 438, 1132

Sugerman, B. E. K. 2003, AJ, 126, 1939

Tylenda, R., Soker, N., & Szczerba, R. 2005, A&A, 441, 1099

Xu, J., Crotts, A. P. S., & Kunkel, W. E. 1994, ApJ, 435, 274

Xu, J., Crotts, A. P. S., & Kunkel, W. E. 1995, ApJ, 451, 806

Date	ZPT Mag.	FWHM	Ecc.	Date	ZPT Mag.	FWHM	Ecc.
011113	31.736	4.31	0.371	041017	31.578	4.64	0.377
011115	31.702	3.65	0.232	041019	31.530	4.18	0.217
011117	31.678	3.79	0.401	041021	31.586	3.18	0.397
011122	31.872	3.96	0.488	041106	31.513	4.52	0.275
011211	31.838	3.11	0.347	041112	31.215	3.32	0.309
011219	31.771	3.54	0.504	041116	31.532	3.45	0.248
011221	31.772	3.44	0.376	041118	31.537	3.71	0.260
020107	31.833	3.28	0.201	041120	31.531	3.42	0.374
020112	31.271	3.57	0.369	041205	31.563	3.41	0.324
020216	31.324	5.12	0.244	041209	31.606	3.54	0.404
020216	31.324	5.12	0.244	041213	31.565	2.93	0.467
020930	31.876	4.52	0.283	041215	31.473	3.68	0.250
021008	31.870	4.51	0.127	041219	31.450	3.44	0.308
021012	31.817	4.29	0.397	041221	31.594	3.68	0.298
021030	31.922	3.93	0.474	050107	31.539	3.34	0.400
021111	31.900	3.60	0.472	050111	31.452	4.19	0.363
021128	31.882	4.25	0.256	050113	31.405	2.85	0.494
021206	31.498	4.95	0.289	050117	31.522	3.49	0.444
021214	31.918	4.32	0.409	050214	31.551	3.82	0.358
021216	31.879	4.62	0.261	050926	31.405	3.49	0.402
031020	31.872	3.90	0.540	051006	31.159	3.95	0.309
031203	31.875	3.99	0.477	051009	31.322	3.98	0.355
031212	31.862	4.44	0.499	051110	31.563	3.17	0.324
031215	31.834	3.88	0.435	051130	31.541	3.39	0.177
031217	31.762	4.57	0.371	051202	31.621	4.05	0.323
031225	31.871	4.46	0.549	051231	31.485	3.07	0.301

Table 1: Selected images of SN 1987A for NN2 analysis with zero-point magnitude and the average FWHM and eccentricity of the point-spread functions. The date format is YYMMDD.

	ρ (pc)	z (pc)
Ring 1	34.3	130
Ring 2	54.0	326
Ring 3	76.1	646
Ring 4	92.6	960
Ring 4 arclet*	106 pc	1260 pc

Table 2: Geometric data for rings in season 2001-2002, calculated as described in section 4. (*Estimate for an arclet in southwestern quadrant.)

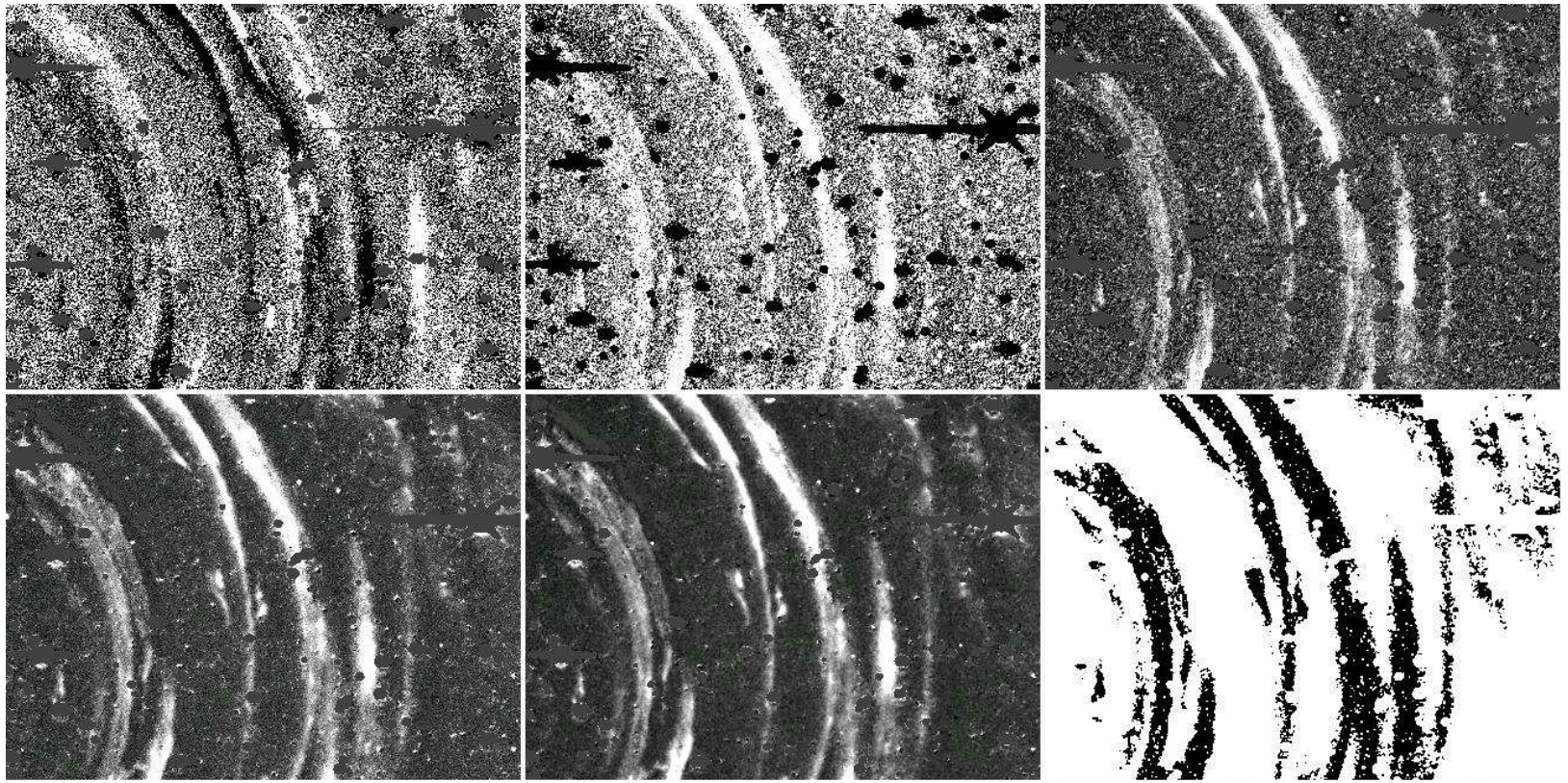

Fig. 1.— Stages of image processing showing strong light echoes. Numbering from left to right, top to bottom. North is up, east is left. (1) Difference image from the SuperMACHO pipeline. White pixels have higher values in the image epoch, and black pixels have higher values in the template epoch. (2) Output from NN2 algorithm for a single epoch. (3) Zero-flux corrected image. (4) Mean-combined image for 2001-2002 season. (5) Smoothed mean-combined image. (6) Detected light echoes. The small holes are around star centers. Images (1)-(5) are shown with the same scales, with the exception of the scale of (2) being shifted upward to account for the lack of negative values in NN2 output. (The zero-flux level is set to the lowest value reached for each pixel.)

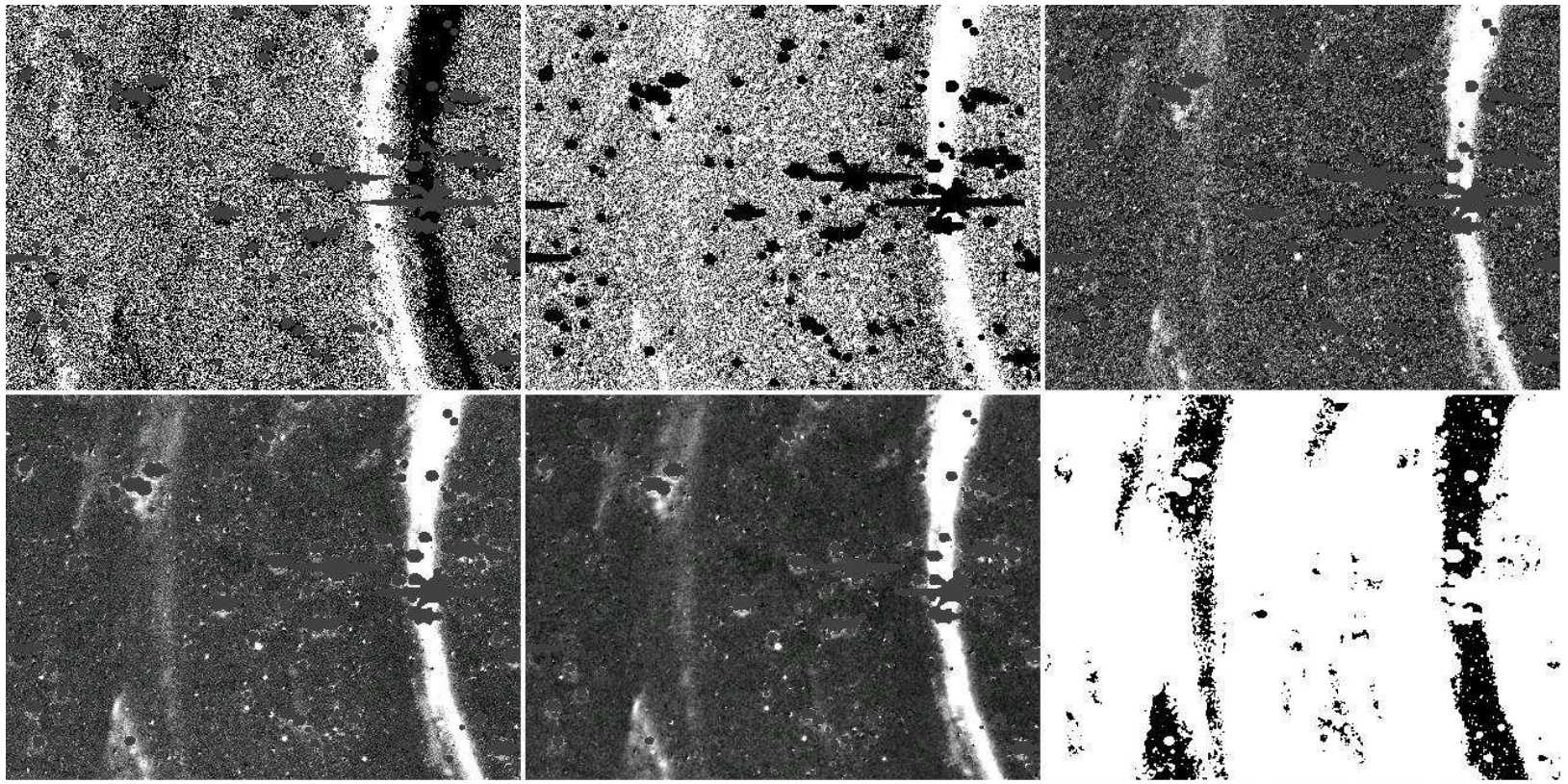

Fig. 2.— Stages of image processing showing weak light echoes. Numbering from left to right, top to bottom. North is up, east is left. Images are from the same epochs as in figure 1. (1) Difference image. (2) Output from NN2 algorithm for a single epoch. (3) Zero-flux corrected image. (4) Mean-combined image for 2001-2002 season. (5) Smoothed mean-combined image. (6) Detected light echoes. Pixels around very bright stars that are unmasked are detected and must be excluded by hand. Each image has the same scale as its counterpart in figure 1.

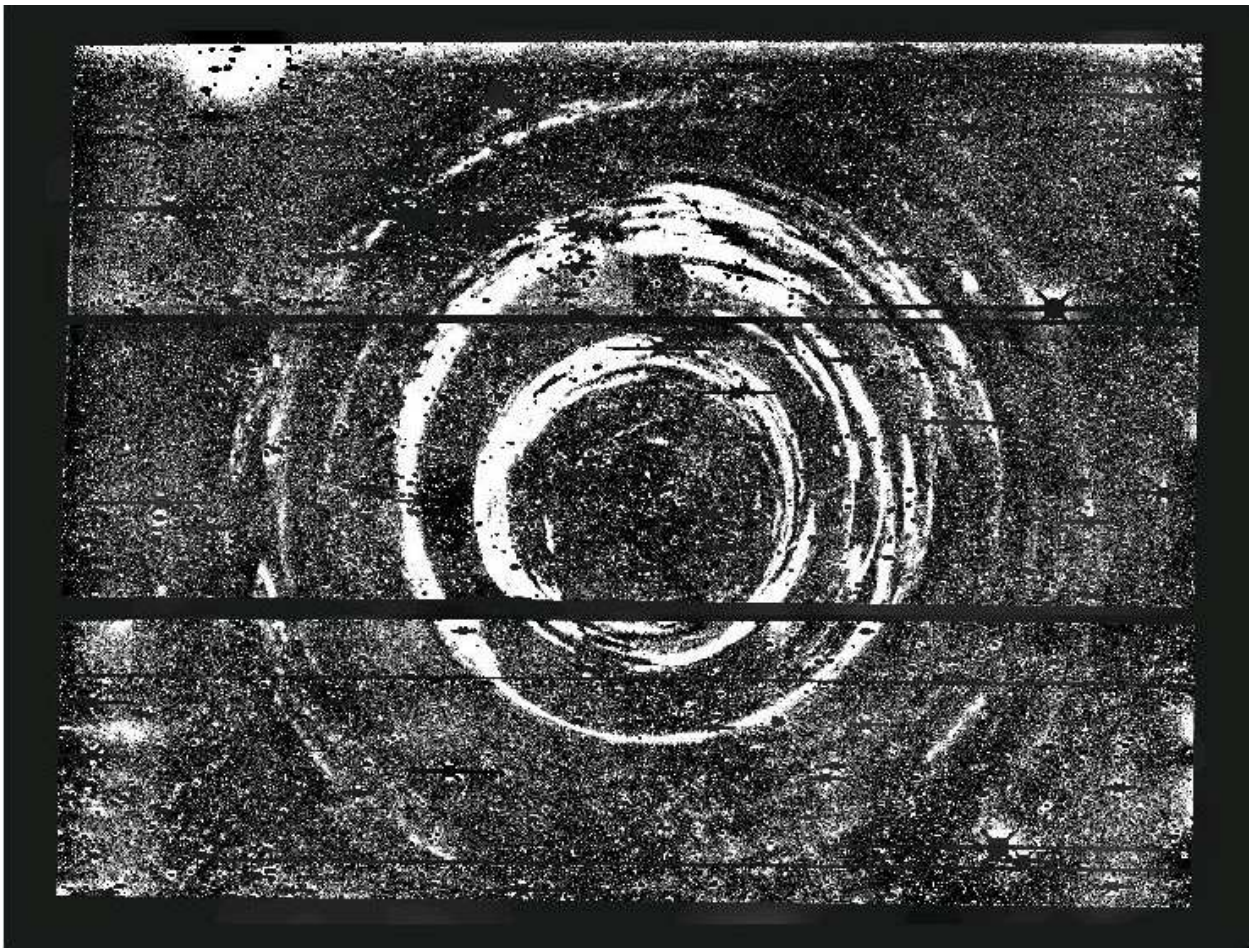

Fig. 3.— Stacked and smoothed image for 2002-2003 season assembled from amplifiers 14, 15, and 16 in field sm77. The field is approximately $18' \times 13.5'$.

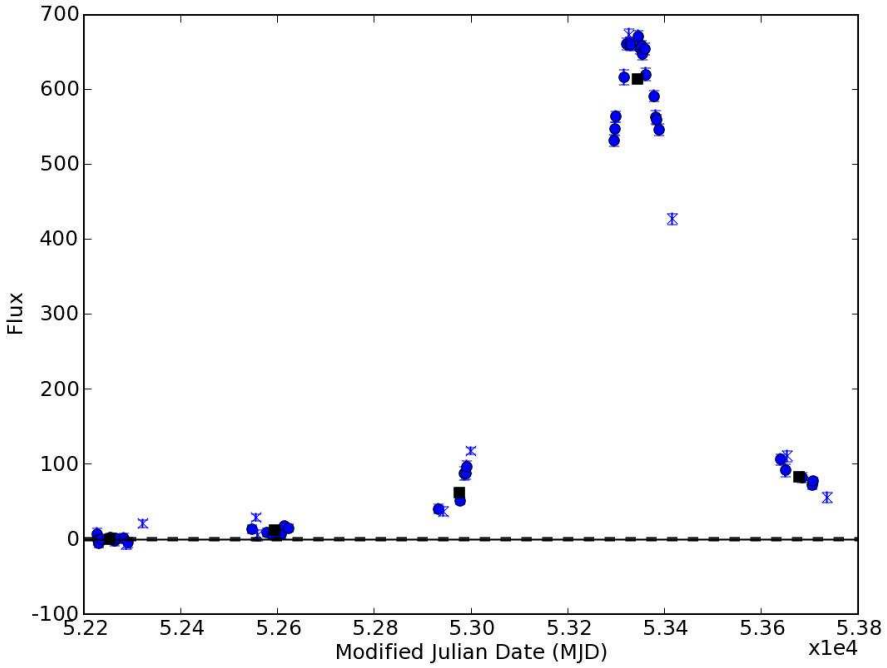

Fig. 4.— Light curve for a pixel containing a strong light echo. Squares denote the season mean fluxes. The minimum and maximum fluxes in each season are excluded from the mean calculation and are denoted by "x" symbols. Seasons 2 through 5 are excluded by the sigma cut, and the zero flux is determined by the mean of the first season.

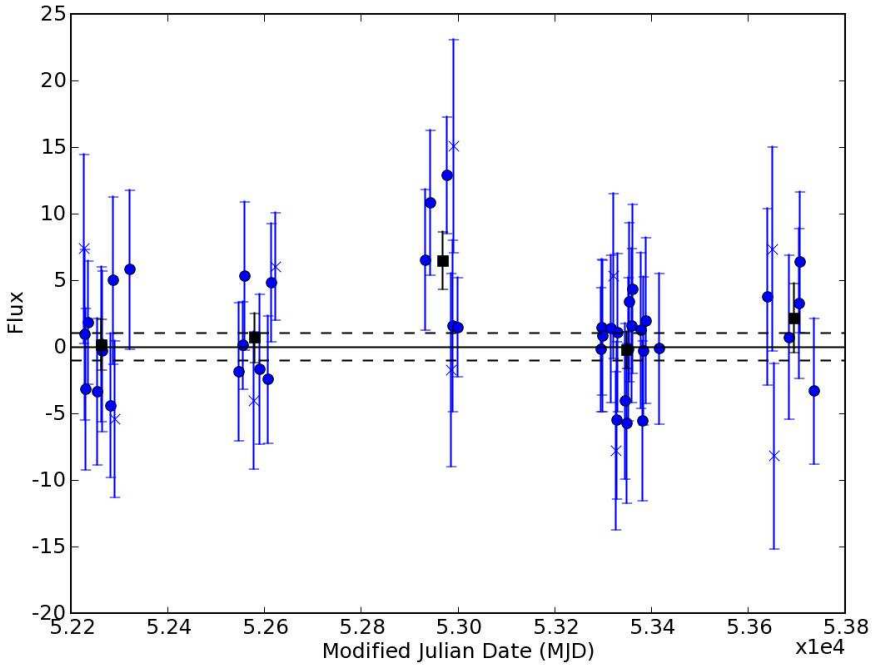

Fig. 5.— Light curve for a pixel containing a weak light echo in season 3 with a peak season-mean surface brightness of 25.2 mag arcsec^{-2}. The zero-flux level is determined by seasons 1, 2, 4, and 5. The dashed lines indicate the 1 σ error in the mean.

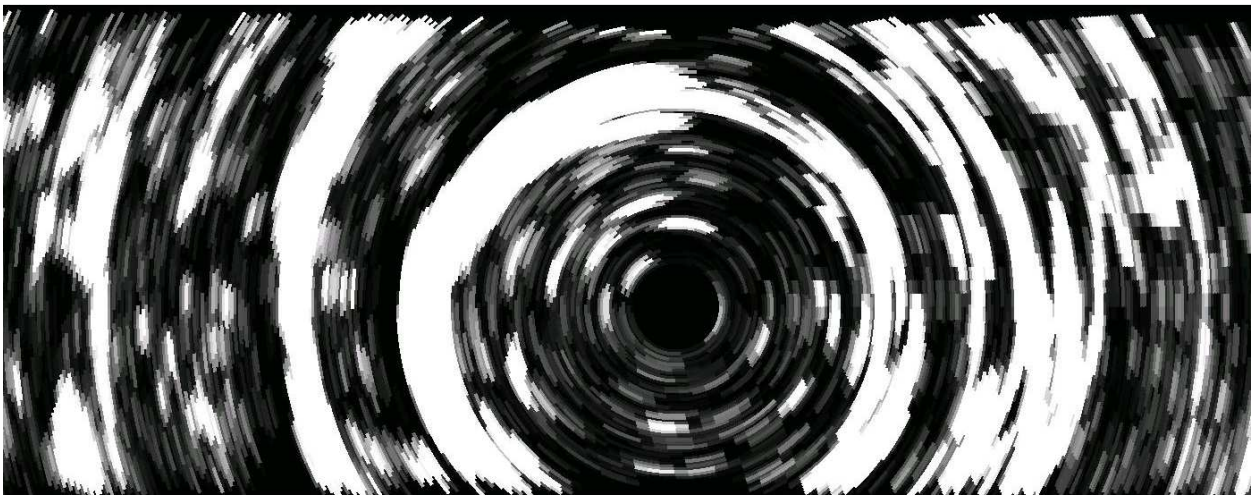

Fig. 6.— Arc association map for selected region around SN 1987A. Pixel values indicate the density of light echo candidates within arclet regions.

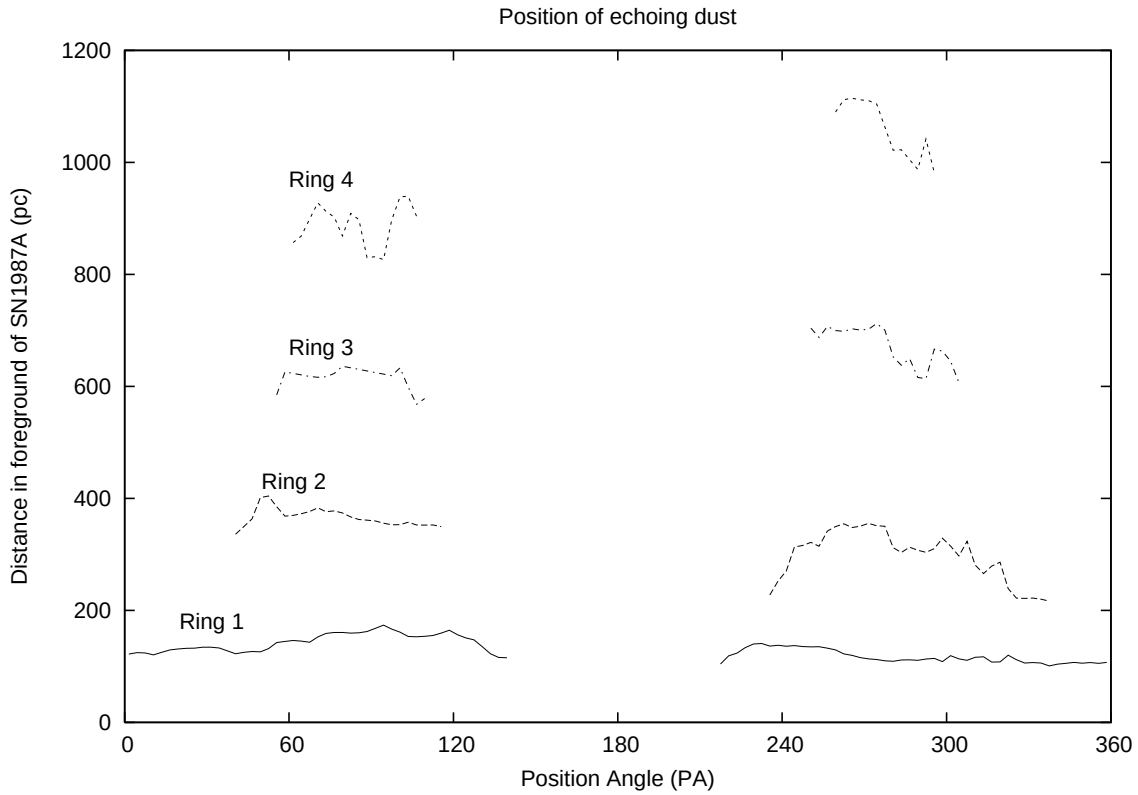

Fig. 7.— Position of echoing dust in 4 rings. Calculated from the mean-combined image for the 2001-2002 season using equation 13 and a flux-weighted mean radius. (Some ranges of position angle are missing because upper and lower regions of light echo arcs were not included in the calculation at the time of this writing.)